Efficiency at maximum power and efficiency fluctuations in a linear Brownian heat-engine model

Jong-Min Park,[1] Hyun-Myung Chun,[1] and Jae Dong Noh[1,2]
[1]*Department of Physics, University of Seoul, Seoul 02504, Korea*
[2]*School of Physics, Korea Institute for Advanced Study, Seoul 02455, Korea*
(Received 24 March 2016; published 19 July 2016)

We investigate the stochastic thermodynamics of a two-particle Langevin system. Each particle is in contact with a heat bath at different temperatures T_1 and T_2 ($<T_1$), respectively. Particles are trapped by a harmonic potential and driven by a linear external force. The system can act as an autonomous heat engine performing work against the external driving force. Linearity of the system enables us to examine thermodynamic properties of the engine analytically. We find that the efficiency of the engine at maximum power η_{MP} is given by $\eta_{MP} = 1 - \sqrt{T_2/T_1}$. This universal form has been known as a characteristic of endoreversible heat engines. Our result extends the universal behavior of η_{MP} to nonendoreversible engines. We also obtain the large deviation function of the probability distribution for the stochastic efficiency in the overdamped limit. The large deviation function takes the minimum value at macroscopic efficiency $\eta = \bar{\eta}$ and increases monotonically until it reaches plateaus when $\eta \leqslant \eta_L$ and $\eta \geqslant \eta_R$ with model-dependent parameters η_R and η_L.

DOI: 10.1103/PhysRevE.94.012127

I. INTRODUCTION

Heat engines are devices to generate mechanical work by exploiting heat flows between hot and cold heat baths at temperatures T_1 and T_2 ($<T_1$). Since the advance of stochastic thermodynamics, Brownian heat engines consisting of microscopic small components have been attracting a great deal of theoretical and experimental interest. Those engines work in nonequilibrium conditions and are subject to large thermal fluctuations. Much efforts have been devoted to understanding common properties that are shared by a variety of different engine models.

The efficiency η, defined as the ratio of the work to the absorbed heat from a hot heat bath, is one of the most important characteristics of a heat engine. According to the laws of thermodynamics, the efficiency is limited from above by the Carnot efficiency $\eta_C \equiv 1 - T_2/T_1$. The Carnot efficiency is achieved only when an engine operates infinitely slow and reversibly. Hence, an engine operating at the Carnot efficiency is of no practical importance because its power, i.e., work per unit time, is zero.

Instead of optimizing the efficiency, researchers are interested in the efficiency of an engine when it is optimized to yield the maximum power, which is called the efficiency at maximum power (EMP) η_{MP}. The EMP is shown to be universal for endoreversible engines that operate reversibly except when they exchange heats with external heat baths [1]. The EMP of the endoreversible engines is given by $\eta_{MP} = \eta_{CA} \equiv 1 - \sqrt{T_2/T_1}$. This efficiency η_{CA} is called the Curzon-Ahlborn efficiency since it was rediscovered by Curzon and Ahlborn [1], although it had been known long before [2,3].

Most of realistic engines are not endoreversible [4,5]. Nevertheless, the EMP of many engines is close to η_{CA} when T_1 and T_2 are close to each other, so $\eta_C \ll 1$. In this limit, the Curzon-Ahlborn efficiency is expanded as $\eta_{CA} = 1 - \sqrt{1-\eta_C} = \frac{1}{2}\eta_C + \frac{1}{8}\eta_C^2 + O(\eta_C^3)$. Some engines, which are not endoreversible, share the same expansion up to first or second order in η_C [6–32]. It was found that the first-order term reflects the tight coupling between thermodynamic fluxes [33] and the second-order term the left-right symmetry [34]. The universality of the expansion has been investigated in the context of irreversible thermodynamics [35].

When one measures the efficiency of an engine for a time interval t, it varies from one measurement to another due to thermal fluctuations. Thus, the efficiency is a fluctuating random variable characterized by the probability distribution function $P_t(\eta)$ and the large deviation function $L(\eta) \equiv -\lim_{t\to\infty} \frac{1}{t} \ln P_t(\eta)$ in the long time limit. Recently, it was found that the large deviation function $L(\eta)$ is maximum at $\eta = \eta_C$. This means that the Carnot efficiency is least likely in the $t \to \infty$ limit. To be precise, such a property was proved for a heat engine that has only a finite number of microscopic configurations and is driven by a time-symmetric protocol [36,37]. The least likeliness of the Carnot efficiency was demonstrated in two-level systems analytically and numerically. However, it remains an open question whether it is valid for systems with continuous variables.

In this paper we introduce an exactly solvable model for a Brownian heat engine. The model consists of two Brownian particles in one dimension that are trapped by a harmonic potential and driven by a linear external force. Each particle is in contact with a heat bath at different temperatures. The temperature difference induces a heat flow, which enables the system to work against the external force. Owing to solvability, the linear systems have been adopted for detailed study of various subjects in stochastic thermodynamics such as entropy production, fluctuation theorems, and information engines [38–41]. We will investigate thoroughly the linear model in terms of the heat engine with the focus on the efficiency of the heat engine. Our results can be summarized as follows. (i) The exact expressions for the macroscopic efficiency and power are derived. We find that the EMP is equal to η_{CA}. Our engine model operates in a nonequilibrium condition, hence it is not an endoreversible engine. This result indicates that endoreversibility is not a necessary condition for $\eta_{MP} = \eta_{CA}$. (ii) The large deviation function $L(\eta)$ for the efficiency is obtained analytically. The function is minimum at the macroscopic efficiency, increases monotonically as η departs from the macroscopic efficiency, and reaches constant

plateaus in the regions with $\eta \geqslant \eta_R$ and $\eta \leqslant \eta_L$. The large deviation function does not have a peak at the Carnot efficiency, which is in sharp contrast to the property of finite-configuration heat engines.

This paper is organized as follows. We introduce the model system and calculate the steady-state average of the heat and work in Sec. II. We elaborate on the EMP and compare it with η_{CA} in Sec. III. In Sec. IV we derive the exact expression for the large deviation function for the efficiency. We summarize our results in Sec. V.

II. LINEAR ENGINE MODEL

We consider a system consisting of two Brownian particles of mass m in one dimension. Two particles are in contact with two different heat baths at temperatures T_1 and T_2 ($<T_1$), respectively, and linear forces are applied. Their motions are governed by the underdamped Langevin equations

$$\begin{aligned} \dot{x}_1 &= v_1, \quad \dot{x}_2 = v_2, \\ m\dot{v}_1 &= -\gamma v_1 - Kx_1 + \epsilon x_2 + \xi_1(t), \\ m\dot{v}_2 &= -\gamma v_2 - Kx_2 + \delta x_1 + \xi_2(t), \end{aligned} \tag{1}$$

where x_i and v_i are the position and the velocity of ith particle (where $i = 1,2$), respectively, γ is a damping coefficient, K is a stiffness constant of a harmonic potential trapping the particles at the origin, (ϵ,δ) are the coupling constants, and $\xi_i(t)$ is the Gaussian-distributed random force satisfying $\langle \xi_i(t)\rangle = 0$ and $\langle \xi_i(t)\xi_j(t')\rangle = 2\gamma k_B T_i \delta_{ij}\delta(t-t')$. We use shorthand notation $\dot{}$ for a time derivative and set the Boltzmann constant k_B to be unity hereafter.

The two-particle system may be interpreted as a single-Brownian-particle system in two dimensions with position column vector $\boldsymbol{x} = (x_1,x_2)^{\mathsf{T}}$ and velocity column vector $\boldsymbol{v} = (v_1,v_2)^{\mathsf{T}} = \dot{\boldsymbol{x}}$. The superscript T stands for the transpose. In this interpretation, the total applied force $\boldsymbol{f}$ is decomposed into the sum of two parts $\boldsymbol{f} = \boldsymbol{f}_c + \boldsymbol{f}_{nc}$, with the conservative force

$$\boldsymbol{f}_c = -K\boldsymbol{x} = -\boldsymbol{\nabla} V(\boldsymbol{x}), \tag{2}$$

with a harmonic potential $V(\boldsymbol{x}) = \frac{1}{2}K\boldsymbol{x}^2$ and the nonconservative driving force

$$\boldsymbol{f}_{nc} = (\epsilon x_2, \delta x_1)^{\mathsf{T}}, \tag{3}$$

which does not have a corresponding potential function unless $\epsilon = \delta$. The motions along the x_1 axis and the x_2 axis are affected independently by the heat baths of temperatures T_1 and T_2, respectively.

For appropriate choices of ϵ and δ, the system can work against the nonconservative force by exploiting the heat flow between the heat baths. Thus it can act as a heat engine as well as a heat pump or a refrigerator. According to stochastic energetics [42], the heat absorbed from the heat baths into the system and the work done by the system against the driving force during an infinitesimal time interval $[t,t+dt]$ are given by

$$\begin{aligned} đ Q_1(t) &= v_1(t) \circ [-\gamma v_1(t)dt + d\Xi_1(t)], \\ đ Q_2(t) &= v_2(t) \circ [-\gamma v_2(t)dt + d\Xi_2(t)], \\ đ W(t) &= -\boldsymbol{f}_{nc} \circ d\boldsymbol{x} = -[\epsilon v_1(t)x_2(t) + \delta x_1(t)v_2(t)]dt, \end{aligned} \tag{4}$$

where $d\Xi_i(t) \equiv \int_t^{t+dt} dt' \xi_i(t')$ are Gaussian random variables satisfying $\langle d\Xi_i(t)\rangle = 0$ and $\langle d\Xi_i(t) d\Xi_j(t)\rangle = 2\gamma T_i \delta_{ij} dt$. The notation $\circ$ represents the Stratonovich product [43,44]. Those quantities satisfy the energy conservation $dE(t) = đ Q_1(t) + đ Q_2(t) - đ W(t)$ with the internal energy $E = \frac{1}{2}m\boldsymbol{v}^2 + V(\boldsymbol{x})$.

We focus on the average quantities in the steady state, denoted by $\langle\cdot\rangle_s$. Fluctuations are considered later. The steady-state average of the internal energy change $\langle dE\rangle_s$ vanishes. Hence, there exist only two relevant quantities describing the energy flow. We choose the heat flow rate from the hot reservoir $q_1 \equiv \langle đ Q_1/dt\rangle_s$ and the work production rate $w \equiv \langle đ W/dt\rangle_s$. The Stratonovich algebra yields that $\langle v_1(t) \circ d\Xi_1(t)\rangle_s = \langle \frac{1}{2}[v_1(t) + v_1(t+dt)] d\Xi_1(t)\rangle_s = \frac{\gamma T_1}{m}dt + o(dt)$. Thus, we obtain the expressions [41,45–47]

$$\begin{aligned} q_1 &= \frac{2\gamma}{m}\left(\frac{T_1}{2} - \frac{1}{2}m\langle v_1^2\rangle_s\right), \\ w &= -\epsilon\langle v_1 x_2\rangle_s - \delta\langle x_1 v_2\rangle_s. \end{aligned} \tag{5}$$

The average heat flux from the cold reservoir is given by $q_2 \equiv \langle đ Q_2/dt\rangle_s = w - q_1$.

The Langevin equations in (1) are linear in $\boldsymbol{z} = (x_1,x_2,v_1,v_2)^{\mathsf{T}}$ and belong to the class of the multivariate Ornstein-Uhlenbeck process [43,44]. In such a case, the steady state is Gaussian distributed with the covariance matrix $\Sigma = \langle \boldsymbol{z}\boldsymbol{z}^{\mathsf{T}}\rangle_s$ being determined as a solution of a set of linear equations. Following the standard procedure (see Sec. 4.5.6 of Ref. [44]), we obtain that

$$\Sigma = \begin{pmatrix} \frac{(K\psi+\gamma^2\phi)}{\delta} & \psi & 0 & \gamma\phi \\ \psi & \frac{(K\psi-\gamma^2\phi)}{\epsilon} & -\gamma\phi & 0 \\ 0 & -\gamma\phi & \frac{T_1}{m} - \epsilon\phi & 0 \\ \gamma\phi & 0 & 0 & \frac{T_2}{m} + \delta\phi \end{pmatrix}, \tag{6}$$

with $\psi = \frac{\delta T_1 + \epsilon T_2}{2(K^2 - \epsilon\delta)}$ and $\phi = \frac{\delta T_1 - \epsilon T_2}{2(\gamma^2 K + m\epsilon\delta)}$. Using the covariance matrix, we find that

$$\begin{aligned} q_1 &= \gamma\epsilon\phi = \frac{\gamma\epsilon(\delta T_1 - \epsilon T_2)}{2(\gamma^2 K + m\epsilon\delta)}, \\ w &= \gamma(\epsilon - \delta)\phi = \frac{\gamma(\epsilon-\delta)(\delta T_1 - \epsilon T_2)}{2(\gamma^2 K + m\epsilon\delta)}. \end{aligned} \tag{7}$$

The covariance matrix is positive definite in the region

$$-\frac{\gamma^2 K}{m} < \epsilon\delta < K^2. \tag{8}$$

Outside the region, the nonconservative force is so strong that the particle escapes from the harmonic potential. The nonconservative force drives the particle to rotate around the potential center generating a centrifugal force in a rotating frame (negative $\epsilon\delta$ case) or blows the particle away from the potential center (positive $\epsilon\delta$ case). Hence, instability occurs when $|\epsilon\delta|$ is large. Mathematically, the stability condition can be also derived from linear stability analysis of the deterministic part of (1). We will restrict ourselves to the stable region for further analysis.

III. EFFICIENCY AT MAXIMUM POWER

As one varies ϵ and δ within the stable region, q_1 and w flip their signs. There are four different regions. (i) When $q_1 > 0$

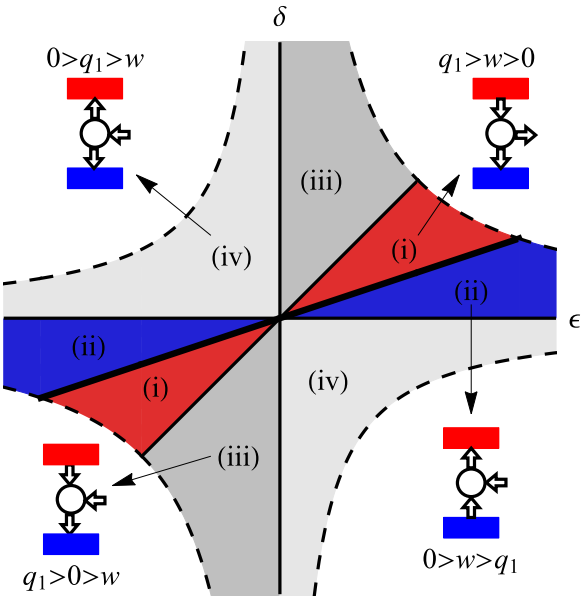

FIG. 1. Function diagram of the linear engine model. The dashed lines are the boundary of the stable region.

and $w > 0$, the system operates as a heat engine that absorbs heat from the hot bath, dissipates heat to a cold bath, and works against the driving force. The macroscopic efficiency is given by

$$\bar{\eta} = \frac{w}{q_1} = 1 - \frac{\delta}{\epsilon}. \tag{9}$$

We use the notation $\bar{\eta}$ for the macroscopic efficiency in order to distinguish it from the stochastic efficiency η investigated later. (ii) When $q_1 < 0$, $w < 0$, and $q_2 = w - q_1 > 0$, the system operates as a heat pump or a refrigerator that transfers heat from the cold bath (q_2) to the hot bath ($|q_1|$) with the help of external work ($|w|$). (iii) When $q_1 > 0$, $w < 0$, and $q_2 < 0$, heat flows from the hot bath to the cold bath at the expense of external work. (iv) When $q_1 < 0$, $w < 0$, and $q_2 < 0$, external work is dissipated into the two baths. The borderlines of these four regions and the stable region are drawn in Fig. 1. The two regions (iii) and (iv) are of no practical importance. We focus on the heat engine region (i).

The regions (i) and (iii) are separated by the line $\delta = \epsilon$, where the force $\boldsymbol{f}_{nc}$ becomes a conservative one. Hence the power w vanishes and the system plays the role of a heat conductor.

The heat engine regime (i) is separated from the heat pump regime (ii) by the line $\delta = (T_2/T_1)\epsilon = (1-\eta_C)\epsilon$, drawn with the thick line in Fig. 1. Along this line, the efficiency in (9) is given by the Carnot efficiency $\eta_C = 1 - T_2/T_1$ with vanishing power [see (7)]. In macroscopic thermodynamics, the Carnot efficiency is achieved only when an engine operates quasistatically and reversibly. The vanishing power and the Carnot efficiency along the line are thus consistent with each other [6,8,12]. In fact, our model can be shown to be in effective thermal equilibrium along the line $\delta = (1-\eta_C)\epsilon$. In terms of dimensionless parameters $\tilde{x}_1 = \frac{x_1}{(\sqrt{mT_1}/\gamma)}$, $\tilde{x}_2 = \frac{x_2}{(\sqrt{mT_2}/\gamma)}$, and $\tilde{t} = \frac{t}{(m/\gamma)}$, the Langevin equation (1) becomes

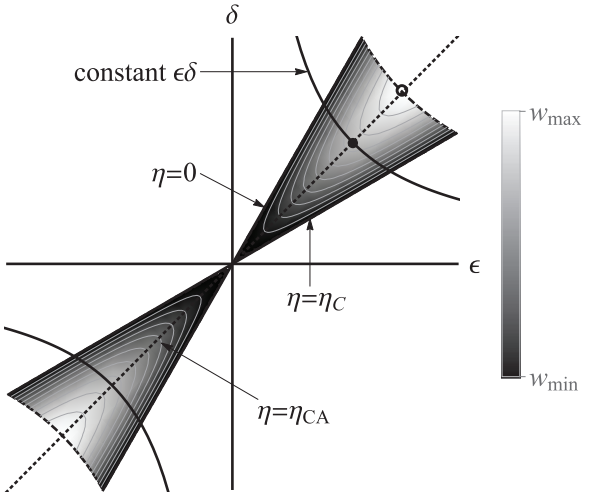

FIG. 2. Density and contour plots for the engine power w.

equivalent to that for a two-dimensional Brownian particle in thermal contact with a single heat bath at unit temperature. The particle is driven by the effective nonconservative force $\tilde{\boldsymbol{f}}_{nc} = (\frac{m}{\gamma^2}\sqrt{\frac{T_2}{T_1}}\epsilon\tilde{x}_2, \frac{m}{\gamma^2}\sqrt{\frac{T_1}{T_2}}\delta\tilde{x}_1)^{\mathsf{T}}$, which turns into the conservative force along the line $\delta = (T_2/T_1)\epsilon = (1-\eta_C)\epsilon$. The temperature difference ($T_1 \neq T_2$) and the nonconservative force $\boldsymbol{f}_{\rm nc}$ are the ingredients that drive the system out of equilibrium. When $\delta T_1 = \epsilon T_2$, their effects cancel each other and the system becomes equivalent to an equilibrium system with an effective temperature.

The power w of the engine varies in the (ϵ,δ) plane as shown in Fig. 2. We will find the maximum power point and investigate how the EMP depends on the temperatures. The power w is given by a function of ϵ and δ in (7). Recalling that the macroscopic efficiency $\bar{\eta}$ in (9) is a function of δ/ϵ, we find it convenient to write w as a function of $\epsilon\delta$ and $\bar{\eta}$ instead of a function of ϵ and δ:

$$w(\epsilon\delta,\bar{\eta}) = \frac{\gamma\epsilon\delta T_1}{2(\gamma^2 K + m\epsilon\delta)}\frac{\bar{\eta}(\eta_C - \bar{\eta})}{1-\bar{\eta}}, \tag{10}$$

with $\eta_C = 1 - T_2/T_1$. Then, for a given $\epsilon\delta$, the power is maximum when $\frac{\partial w}{\partial \bar{\eta}} = 0$, which yields that

$$\eta_{MP} = 1 - \sqrt{1-\eta_C}. \tag{11}$$

This is the EMP along the constant-$\epsilon\delta$ curves (see Fig. 2). The global maximum of the power is achieved in the limiting case where $\epsilon\delta$ approaches K^2, the border of the stable region [see (8)], the efficiency at which is also given by (11).

To our surprise, the result for the efficiency at maximum power is the same as the Curzon-Ahlborn efficiency η_{CA} obtained for the endoreversible engine [1]. It reveals that the endoreversibility is not a necessary condition for $\eta_{MP} = \eta_{CA}$. In order to understand the similarity between our model and the endoreversible engines, we rederive the Curzon-Ahlborn result [1,48,49]. An endoreversible engine operates under the assumption that it maintains internal temperatures T_{1i} and T_{2i} when it exchanges heat with the heat baths at temperatures at T_1 and T_2, respectively. The endoreversibility means that the engine operates as the Carnot engine between two temperatures T_{1i} and T_{2i}. Assuming the Fourier law, the

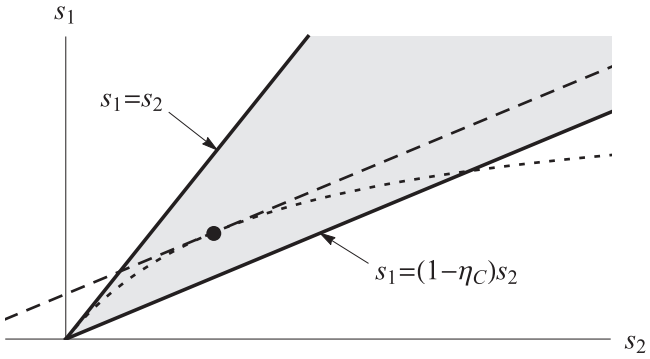

FIG. 3. Linear heat engine model in the (s_1,s_2) plane. The model acts as a heat engine in the shaded area satisfying $(1-\eta_C)s_2 < s_1 < s_2$. The dotted curve represents a characteristic of the engine. The maximum power is achieved when the curve is tangential to a straight line of slope $1-\eta_C$.

incoming (q_1) and outgoing $(-q_2)$ heat fluxes are given by $q_1 = \alpha_1(T_1 - T_{1i})$ and $-q_2 = \alpha_2(T_{2i} - T_2)$, respectively, with the heat conductivities α_i. Then the endoreversible condition amounts to $q_1/T_{1i} = -q_2/T_{2i}$. The power is given by $w = q_1 + q_2 = \alpha_1(T_1 - T_{1i}) - \alpha_2(T_{2i} - T_2)$. It is a function of the internal temperatures T_{1i} and T_{2i}, which are determined by an operating condition. Using the endoreversible condition and the expression for the efficiency $\bar{\eta} = 1 - \frac{\alpha_2(T_{2i}-T_2)}{\alpha_1(T_1-T_{1i})}$, one can eliminate T_{1i} and T_{2i} in w to obtain that

$$w = \frac{\alpha_1\alpha_2 T_1}{\alpha_1+\alpha_2}\frac{\bar{\eta}(\eta_C-\bar{\eta})}{1-\bar{\eta}}. \tag{12}$$

Apart from the overall factor, it has the same $\bar{\eta}$ dependence as in (10), hence the same efficiency at maximum power.

Comparing (10) and (12), one finds that the Curzon-Ahlborn efficiency $\eta_{CA} = 1 - \sqrt{T_2/T_1}$ is a consequence of the specific relation between the thermodynamic quantities irrespective of microscopic details of engines. It is convenient to use the parameters $s_1 = q_1/T_1$ (entropy loss of the hot bath) and $s_2 = -q_2/T_2$ (entropy gain of the cold bath). Using $w = s_1T_1 - s_2T_2$ and $\bar{\eta} = 1 - s_2T_2/s_1T_1$, we can rewrite (10) and (12) in the form $s_1 = \mathcal{F}(s_2)$, where the function $\mathcal{F}(x)$ is given by

$$\mathcal{F}(x) = \frac{x}{1+\zeta x}, \tag{13}$$

with $\zeta = 2(\gamma^2K + m\epsilon\delta)/\gamma\epsilon\delta$ for (10) and $\zeta = \alpha_1^{-1} + \alpha_2^{-1}$ for (12).

In general, as one varies engine-specific parameters, such as ϵ and δ in our model or T_{1i} and T_{2i} in the endoreversible engine, s_1 and s_2 will move along a curve $s_1 = \mathcal{F}(s_2)$. We now address the question whether the function $\mathcal{F}(x)$ in (13) is uniquely determined for all systems displaying the Curzon-Ahlborn efficiency. In Fig. 3 we draw an arbitrary curve (dotted line) in the (s_1,s_2) plane. The second law of thermodynamics $s_1 \leqslant s_2$ requires that the function $\mathcal{F}(x)$ should be below the straight line $s_1 = s_2$. The device works as a heat engine when $s_1 > 0$, $s_2 > 0$, and $w = q_1 + q_2 = T_1s_1 - T_2s_2 \geqslant 0$. Hence, the shaded area between two straight lines $s_1 = s_2$ and $s_1 = (T_2/T_1)s_2 = (1-\eta_C)s_2$ is the region of physical interest. Noting that the power of the engine is constant along a straight line $s_1 = (1-\eta_C)s_2 + w/T_1$, one finds that the maximum power achieved when the curve $s_1 = \mathcal{F}(s_2)$ is tangential to the straight line of slope $1-\eta_C$. The tangential point (s_1^*,s_2^*), hence the maximum power point, is determined by

$$s_1^* = \mathcal{F}(s_2^*), \quad (1-\eta_C) = \mathcal{F}'(s_2^*). \tag{14}$$

The efficiency at maximum power is then given by

$$\eta_{MP} = 1 - (1-\eta_C)\frac{s_2^*}{s_1^*}. \tag{15}$$

We now impose that $\eta_{MP} = 1 - \sqrt{1-\eta_C}$ for any combinations for T_1 and T_2, i.e., any value of η_C. Eliminating η_C using (14) and (15), we obtain the differential equation for the function $\mathcal{F}(x)$:

$$\mathcal{F}'(x) = \frac{\mathcal{F}(x)^2}{x^2}. \tag{16}$$

The solution of the differential equation is given by the function in (13). This analysis shows that the Curzon-Ahlborn efficiency at maximum power is achieved if and only if the entropy loss rate in the hot reservoir and the entropy gain rate in the cold reservoir are constrained by the function given in (13).

We add a few remarks. First, there have been attempts to understand the Curzon-Ahlborn efficiency from the symmetry consideration. Near equilibrium where $T_1 \simeq T_2$ or $\eta_C = 1 - T_2/T_1 \ll 1$, the Curzon-Ahlborn efficiency is expanded as $\eta_{CA} = \frac{1}{2}\eta_C + \frac{1}{8}\eta_C^2 + O(\eta_C^3)$. The first-order term $\frac{1}{2}\eta_C$ reflects the tight coupling between thermodynamic fluxes [33]. Namely, the heat fluxes and mechanical flux are proportional to each other, so the total entropy production should also be proportional to the heat flux or s_1. The function form $\mathcal{F}(x) = x/(1+\zeta x)$ implies that the total entropy production rate is given by $s_{\rm tot} = -s_1 + s_2 = \zeta s_1 s_2$, which shows that our model belongs to the tight coupling category. The second-order term $\frac{1}{8}\eta_C^2$ is a manifestation of the so-called left-right symmetry [34] under the exchange of the role between the hot and cold heat baths. Note that the relation $s_1 = \mathcal{F}(s_2)$ is invariant under the changes $s_1 \to -s_2$ and $s_2 \to -s_1$ because the inverse of $\mathcal{F}(x)$ is given by $\mathcal{F}^{-1}(x) = -\mathcal{F}(-x)$. Thus, our model has the left-right symmetry. The higher-order terms do not have a simple explanation yet. Hopefully, our result will shed light on the physical meaning of all the higher-order terms.

Second, in general, as one varies microscopic parameters, an engine may cover the whole physical region in the (s_1,s_2) plane instead of following a one-dimensional curve such as $s_1 = \mathcal{F}(s_2)$ in our model. Such a one-dimensional representation is possible when there exist only a single independent parameter. The model of Curzon and Ahlborn includes two parameters T_{1i} and T_{2i} [1]. However, the endoreversibility condition eliminates one degree of freedom. In our model we reduced the number of independent parameters by following the constant $\epsilon\delta$ curve. For general heat engines with multiple degrees of freedom, if the entropy production rates of two reservoirs satisfy $s_1 = \mathcal{F}(s_2)$ with a certain parameter ζ, the efficiency at maximum power at constant ζ is always given by η_{CA}. It raises questions on the universality of η_{CA} and on the role of such a parameter ζ, which are beyond the scope of the present study.

IV. EFFICIENCY FLUCTUATION

The efficiency η is a fluctuating random variable. Recent studies suggest that it is least probable that a nonequilibrium heat engine would achieve the Carnot efficiency $\eta_C = 1 - T_2/T_1$ in the long time limit [36,37]. This result is derived for an engine that possesses a finite number of microscopic states and is driven by a time-symmetric protocol. Our engine is driven by a time-independent protocol that is obviously time symmetric. However, its phase space is continuous with infinitely many microscopic states. We will examine whether the general statement of Refs. [36,37] is also valid in our model.

For simplicity, we consider the overdamped dynamics. Hereafter, the time will be rescaled so that the damping coefficient is taken to be unity. Then the equations of motion for the position vector $\boldsymbol{x} = (x_1, x_2)^{\mathsf{T}}$ are written as $\dot{\boldsymbol{x}} = \boldsymbol{f} + \boldsymbol{\xi}$, with the force $\boldsymbol{f} = \boldsymbol{f}_c + \boldsymbol{f}_{nc}$ and the thermal noise $\boldsymbol{\xi} = (\xi_1, \xi_2)^{\mathsf{T}}$. Our task is to find the probability distribution $P_t(\eta)$ for the stochastic efficiency $\eta = W/Q_1$, where Q_1 is the heat absorbed from the hot reservoir and W is the work done against the nonconservative force $\boldsymbol{f}_{nc}$ up to time t (we will drop the subscript in Q_1 for notational convenience). We focus on the large deviation function (LDF)

$$L(\eta) \equiv -\lim_{t\to\infty} \frac{1}{t} \ln P_t(\eta). \tag{17}$$

In order to find $P_t(\eta)$, one needs to obtain the joint probability distribution $p(Q, W; t)$. It is accessible by considering the Fokker-Planck equation for the probability distribution $p(\boldsymbol{y}; t)$ of the four-component vector $\boldsymbol{y} = (x_1, x_2, Q, W)^{\mathsf{T}}$. This method was introduced for the heat fluctuation of a one-dimensional Brownian particle [50]. We extend the method to calculate the joint distribution for Q and W. The generating function is defined as

$$G_t(x_1, x_2, \lambda_Q, \lambda_W) \equiv \int dQ\, dW\, e^{-\lambda_Q Q - \lambda_W W} p(\boldsymbol{y}; t). \tag{18}$$

After a lengthy algebra, we find that

$$G_t \propto \exp\left[-\tfrac{1}{2}\boldsymbol{x}^{\mathsf{T}} \cdot \mathsf{D}^{-1/2}\mathsf{J}\mathsf{D}^{-1/2} \cdot \boldsymbol{x} + \mu(\lambda_Q, \lambda_W)t\right] \tag{19}$$

in the large t limit, where $\mathsf{J} = \mathsf{J}(\lambda_Q, \lambda_W)$ is a symmetric 2×2 matrix and

$$\mu(\lambda_Q, \lambda_W) = H(\lambda_Q + \bar{\eta}\lambda_W) \tag{20}$$

with the function

$$H(\Lambda) = K - \sqrt{K^2 + \epsilon^2 T_1 T_2 \left[\Lambda_m^2 - (\Lambda - \Lambda_m)^2\right]}, \tag{21}$$

with

$$\Lambda_m = \frac{\eta_C - \bar{\eta}}{2T_2} \geqslant 0. \tag{22}$$

Here $\bar{\eta} = \langle W\rangle/\langle Q\rangle = 1 - \delta/\epsilon$ is the macroscopic efficiency derived in the previous section and $\eta_C = 1 - T_2/T_1$ is the Carnot efficiency. The derivation and the exact expression for J are presented in the Appendix.

After integrating $G_t(x_1, x_2, \lambda_Q, \lambda_W)$ over $\boldsymbol{x}$, one obtains the reduced generating function $\tilde{G}_t(\lambda_Q, \lambda_W)$ for Q and W. The integration does not introduce an additional t-dependent term in the exponent as far as J is positive definite. Therefore, the cumulant generating function (CGF) $\phi(\lambda_Q, \lambda_W) = \lim_{t\to\infty} \frac{1}{t} \ln \tilde{G}_t(\lambda_Q, \lambda_W)$ [37] is given by

$$\phi(\lambda_Q, \lambda_W) = \mu(\lambda_Q, \lambda_W)\chi_{\mathsf{J}}(\lambda_Q, \lambda_W), \tag{23}$$

where the characteristic function $\chi_{\mathsf{J}}(\lambda_Q, \lambda_W)$ is equal to unity if the matrix $\mathsf{J}(\lambda_Q, \lambda_W)$ is positive definite and infinity otherwise.

The LDF $L(\eta)$ is then obtained by using the relation

$$L(\eta) = -\min_{\lambda} \phi(-\eta\lambda, \lambda), \tag{24}$$

which was derived in Ref. [37]. To a given value of η, one need to evaluate the minimum value of the function $\phi(\lambda_Q, \lambda_W)$ along a straight line l_η of slope $-\eta$ passing through the origin in the $\boldsymbol{\lambda} = (\lambda_W, \lambda_Q)$ plane. Such a task is achieved by using the property of the function μ. Recall that $\mu(\lambda_Q, \lambda_W) = H(\lambda_Q + \bar{\eta}\lambda_W)$ depends on a single parameter $\Lambda = \lambda_Q + \bar{\eta}\lambda_W$. Thus, it is constant along a straight line of slope $-\bar{\eta}$ in the $\boldsymbol{\lambda}$ plane. The function $H(\Lambda)$ has the minimum value

$$\mu_m = K - \sqrt{K^2 + \epsilon^2 T_1 T_2 \Lambda_m^2} \leqslant 0 \tag{25}$$

at $\Lambda = \Lambda_m$ and increases monotonically as Λ deviates from Λ_m. Thus, $L(\eta)$ is determined by the distance of the line l_η and $\Lambda = \Lambda_m$ inside the domain of $\chi_{\mathsf{J}} = 1$.

In Fig. 4 we explain a graphical method to construct $L(\eta)$. This method gives information on the shape of $L(\eta)$: $L(\eta = \bar{\eta}) = 0$, where $L(\eta)$ increases monotonically as η deviates from $\bar{\eta}$ in the region $\eta_L < \eta < \eta_R$ and remains constant $L(\eta) = -\mu_m \geqslant 0$ elsewhere. The boundaries η_L ($\leqslant\bar{\eta}$) and η_R ($\geqslant\bar{\eta}$) vary with the model parameters.

In Fig. 5 we show the plot of $L(\eta)$ obtained from the analytic method using the parameters $K = 1, T_1 = 2, T_2 = 1, \epsilon = 1/2$, and $\delta = 3/8$ with the macroscopic efficiency $\bar{\eta} = 1 - \delta/\epsilon = 1/4$. The LDF takes the minimum value 0 at $\eta = \bar{\eta}$ and a constant value $-\mu_m = (\sqrt{17} - 4)/4$ in the regions with $\eta \leqslant \eta_L \simeq 0.098$ and $\eta \geqslant \eta_R \simeq 0.278$.

We also performed numerical simulations to confirm the analytic result. Starting from the fixed initial configuration $x_1 = x_2 = 0$, we integrated the time-discretized overdamped Langevin equation numerically by using the Heun method [51] with $\Delta t = 0.01$. We measured the work and the heat up to time $t = 512$, 1024, and 2048 and constructed the probability distribution for the efficiency $P_t(\eta)$ by repeating the simulations for $N_s = 3\times2^{25} \approx 10^8$ times. The LDF $L(\eta)$ can be estimated by fitting $-\frac{1}{t}\ln P_t(\eta)$ to the function $A(\eta)/t + B(\eta)\ln t/t + L(\eta)$ at each value of η [52,53]. The LDF thus obtained is presented in Fig. 5. The numerical result is in good agreement with the analytic result: $L(\eta)$ is minimum at $\eta = \bar{\eta}$ and monotonically increases as η deviates from $\bar{\eta}$ to reach its maximum, although statistical uncertainty becomes noticeable for large $|\eta - \bar{\eta}|$.

Also shown in Fig. 5 is the LDF obtained from the steady-state initial condition where x_1 and x_2 at $t = 0$ are drawn from the steady-state distribution. Interestingly, the LDF is different from the LDF obtained from the fixed initial condition. The LDF of nonequilibrium fluctuations may be affected by the initial condition due to the everlasting initial memory effect [54]. Our results exemplify the initial-condition-dependent behavior of the LDF (see also the Appendix).

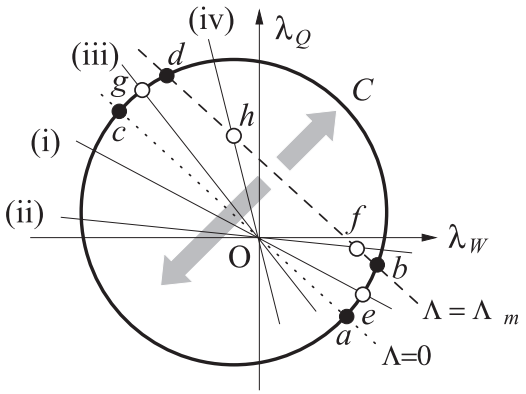

FIG. 4. In the $\boldsymbol{\lambda}=(\lambda_W,\lambda_Q)$ plane, we draw schematically the boundary C of the $\chi_J=1$ domain. The dotted straight line of slope $-\bar{\eta}$ passing through the origin corresponds to the line $\Lambda=0$, while the dashed straight line of slope $-\bar{\eta}$ corresponds to the line $\Lambda=\Lambda_m$, where $\Lambda=\lambda_Q+\bar{\eta}\lambda_W$. The intersections between the line $\Lambda=0$ (Λ_m) and the curve C are marked with closed circles and labeled as a and c (b and d). The gray arrows indicate that the cumulant generating function ϕ in (23) is minimum along the line $\Lambda=\Lambda_m$ and increases as one moves away from it. To a given value of η, $L(\eta)$ is obtained from the minimum value of $\mu(\lambda_Q,\lambda_W)$ along the segment of the straight line l_η passing through the origin O with slope $-\eta$ inside the boundary C. When $\eta=\bar{\eta}$, the line l_η coincides with the line $\Lambda=0$ where $\mu=0$. Hence, $L(\bar{\eta})=0$. (i) When $\eta_L\leqslant\eta<\bar{\eta}$, the right intersection point e (open circle) of l_η and C lies on a segment between a and b. Thus, the LDF is determined by the Λ value at e, $L(\eta)=-H(\Lambda_e)$. The left intersection point is irrelevant since it is farther from the line $\Lambda=\Lambda_m$ than e. The territory η_L is determined by the condition that the point e coincides with b. (ii) When $\eta<\eta_L$, the line l_η intersects with the line $\Lambda=\Lambda_m$ within C at point f (open circle). Hence, $L(\eta)=-\mu_m$. (iii) When $\bar{\eta}<\eta\leqslant\eta_R$, the left intersection point g (open circle) lies on a segment between c and d. Thus, the LDF is given by $L(\eta)=-H(\Lambda_g)$. The territory η_R is determined by the condition that g coincides with d. (iv) When $\eta>\eta_R$, the line l_η intersects with the line $\Lambda=\Lambda_m$ at point h (open circle) and $L(\eta)=-\mu_m$.

The LDF of our model system does not follow the universal behavior, suggested in Refs. [36,37], that the Carnot efficiency is the sole maximum point of the LDF. We briefly review the theory in Refs. [36,37], where the least likeliness of the Carnot efficiency was shown for systems possessing a finite number $\Omega_{\rm sys}$ of microscopic states. The finiteness of $\Omega_{\rm sys}$ plays a crucial role. The total entropy production of the engine and two heat baths is given by $\Delta S_{\rm tot}=-\frac{Q_1}{T_1}-\frac{Q_2}{T_2}+\Delta S_{\rm sys}$ with the Shannon entropy change $\Delta S_{\rm sys}$ of the system. The energy conservation requires that $\Delta E=Q_1+Q_2-W$, where ΔE denotes the change in the internal energy of the engine. Eliminating Q_2, the total entropy production is given by $\Delta S_{\rm tot}=\frac{\eta_C}{T_2}Q_1-\frac{1}{T_2}W+(-\frac{1}{T_2}\Delta E+\Delta S_{\rm sys})$. Note that the mean value of Q_1 and W increases linearly in t. On the other hand, when $\Omega_{\rm sys}$ is finite, $|\Delta E|$ is bounded above by $|E_{\rm max}-E_{\rm min}|$ with the maximum (minimum) energy $E_{\rm max}$ ($E_{\rm min}$) among the $\Omega_{\rm sys}$ states and $|\Delta S_{\rm sys}|$ by $\ln\Omega_{\rm sys}$. Then $\Delta S_{\rm tot}$ may be approximated as $\Delta S_{\rm tot}\simeq\frac{\eta_C}{T_2}Q_1-\frac{1}{T_2}W$ in the large t limit. If the total entropy production is written in the additive form of Q_1 and W, the joint probability distribution

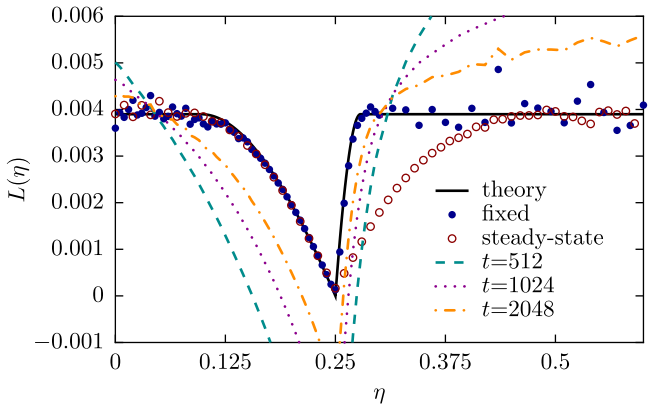

FIG. 5. The LDF for efficiency with the set of parameters $K=1$, $T_1=2$, $T_2=1$, $\epsilon=1/2$, and $\delta=3/8$. The solid line represents the analytic result obtained from Eq. (24), while closed circles represent the numerical results from the fixed initial condition. The numerical results are obtained by extrapolating $-\frac{1}{t}\ln P_t(\eta)$ at $t=512$ (dashed line), 1024 (dotted line), and 2048 (dash-dotted line). Details for the simulations are explained in the text. We also present the numerical results (open circles) that are obtained from the steady-state initial condition.

of them would satisfy the fluctuation theorem [55–58]

$$\frac{P(Q_1,W)}{P(-Q_1,-W)}\simeq e^{\Delta S_{\rm tot}}. \tag{26}$$

It implies that the CGF $\phi(\lambda_Q,\lambda_W)$ should have the symmetry property

$$\phi(\lambda_Q,\lambda_W)=\phi\big(2\lambda_Q^s-\lambda_Q,2\lambda_W^s-\lambda_W\big), \tag{27}$$

with the symmetric point $(\lambda_Q^s,\lambda_W^s)=(\frac{\eta_C}{2T_2},-\frac{1}{2T_2})$. If the CGF has a unique minimum point, (27) means that ϕ takes its global minimum at $(\lambda_Q^s,\lambda_W^s)$. Thus, by using (24), one would find that $L(\eta)\leqslant-\phi(\lambda_Q^s,\lambda_W^s)=L(\eta_C)$ for all η. Namely, the least likeliness of the Carnot efficiency is the direct consequence of the fluctuation theorem and the nondegenerate minimum of the CGF [36,37].

In our model, the fluctuation theorem for $P(Q_1,W)$ is not valid and the CGF $\phi(\lambda_Q,\lambda_W)$ in (23) does not have the symmetry property of (27). Although the averages of $\Delta S_{\rm sys}$ and internal energy change ΔE are zero in the steady state, stochastic fluctuations may generate rare events accompanied by $\Delta S_{\rm sys}$ and ΔE comparable with Q_i and W [59]. Such fluctuations are non-negligible and invalidate the fluctuation theorem [57,58,60].

Despite the breakdown of the fluctuation theorem, the CGF $\phi(\lambda_Q,\lambda_W)=\mu(\lambda_Q,\lambda_W)\chi_J(\lambda_Q,\lambda_W)$ in (23) has an interesting property. The function $\mu(\lambda_Q,\lambda_W)$ depends only on the single parameter $\Lambda=\lambda_Q+\bar{\eta}\lambda_W$ and enjoys the symmetry property $\mu(\lambda_Q,\lambda_W)=\mu(2\lambda_Q^s-\lambda_Q,2\lambda_W^s-\lambda_W)$. At the symmetric point $(\lambda_Q^s,\lambda_W^s)$, Λ is equal to Λ_m and $\mu(\lambda_Q^s,\lambda_W^s)=\mu_m$. It is the characteristic function $\chi_J(\lambda_Q,\lambda_W)$ that breaks the symmetry of (27). As shown in the previous paragraphs, the plateau in $L(\eta)$ originates from the fact that $\phi(\lambda_Q,\lambda_W)$ depends only on Λ within the domain of $\chi_J=1$.

We note that the similar results were reported in Refs. [61,62]. These papers consider the Gaussian fluctuations

of the work and heat using the linear response theory. In the tight coupling limit, Q_1 and W becomes δ-function correlated and the CGF $\phi(\lambda_Q,\lambda_W)$ depends only on a single parameter Λ, a linear combination of λ_Q and λ_W, in the whole (λ_Q,λ_W) space. Consequently, the LDF $L(\eta)$ takes a positive constant value at all values of η except at $\eta=\bar{\eta}$, where $L(\bar{\eta})=0$ [61]. The Carnot efficiency η_C is not least unlikely but equally unlikely as all the values of η other than the macroscopic efficiency $\bar{\eta}$. The plateau in $L(\eta)$ in our model has the same origin as the tight coupling model.

The breakdown of the fluctuation theorem is reflected in the characteristic function χ_{J}. It makes the LDF $L(\eta)$ vary continuously within the interval $\eta_L \leqslant \eta \leqslant \eta_R$, where η_L and η_R are determined by the boundary C of the $\chi_{\mathsf{J}}=1$ domain. The reversible efficiency η_C belongs to the plateau if the symmetry point $(\lambda_Q^s,\lambda_W^s)$ is located inside C. We have examined several different parameter values and found that η_C belongs to the plateau for the fixed initial condition case. When one compares the numerical data in Fig. 5, the deviation from the fluctuation theorem gets stronger and the interval $\eta_L \leqslant \eta \leqslant \eta_R$ becomes broader under the steady-state initial condition. One can imagine a situation where the $\chi_{\mathsf{J}}=1$ domain shrinks so that the symmetric point $(\lambda_Q^s,\lambda_W^s)$ is located outside the domain boundary C. In such a case, the reversible efficiency η_C will belong to the interval $\eta_L \leqslant \eta \leqslant \eta_R$, becoming more likely than other efficiencies. In fact, in a simple model of heat conduction through a Brownian particle in thermal contact with two heat baths, the symmetry for the CGF for the heat imposed by the fluctuation theorem is shown to be broken not only globally but also locally around the symmetric point when the steady-state initial condition is adopted [50]. This example suggests the possibility that $\eta_L < \eta_C < \eta_R$ under the steady-state initial condition. An analytic expression for the CGF under the steady-state initial condition is not available yet. Further work is necessary to investigate whether the breakdown of the fluctuation theorem affects the fluctuations of the efficiency, especially near the reversible efficiency η_C.

V. CONCLUSION

In this paper we introduced a model for a heat engine that operates between two heat baths and is driven by a nonconservative force. The model is described by an Ornstein-Uhlenbeck process and most of the properties are analytically tractable. First, we showed that the efficiency at maximum power is given by the so-called Curzon-Ahlborn efficiency $\eta_{MP}=\eta_{CA}=1-\sqrt{T_2/T_1}$. This is a surprising result because η_{CA} has been believed to be the property of the endoreversible engine, while our engine is not endoreversible. Instead, we showed that η_{CA} is a consequence of the relation $s_1=\mathcal{F}(s_2)$ between the entropy loss s_1 of the hot bath and the entropy gain s_2 of the cold bath with the universal function given in (13).

Second, we derived the analytic expression for the LDF $L(\eta)$ of the efficiency fluctuation. The shape of $L(\eta)$ is shown in Fig. 5: It is minimum at $\eta=\bar{\eta}$ and displays plateaus far from $\bar{\eta}$. Our result shows that $L(\eta)$ does not have a peak at the Carnot efficiency η_C. We also found that the LDF of the efficiency depends on the initial condition, which stresses the initial memory effect of nonequilibrium systems [54].

The linear solvable model has provided a great deal of information on the properties of the heat engines. It also suggests interesting theoretical questions. It is shown that the Curzon-Ahlborn efficiency at maximum power is guaranteed by the relation $s_1=\mathcal{F}(s_2)$ with the universal function $\mathcal{F}(x)$ given in (13). On the other hand, the Curzon-Ahlborn efficiency was investigated in terms of symmetry in Refs. [33–35]. It would be interesting to pursue the implication of the relation $s_1=\mathcal{F}(s_2)$ on underlying symmetry of engine dynamics. The LDF $L(\eta)$ for the system under the steady-state initial condition requires all the eigenstates of the Fokker-Planck operator, which are not available yet. We leave those tasks for future work.

ACKNOWLEDGMENTS

This research was supported by National Research Foundation of Korea Grant No. 2013R1A2A2A05006776. We would like to thank an anonymous referee for useful comments on the tight coupling study.

APPENDIX: DERIVATION OF $L(\eta)$ AND DISCUSSION OF THE INITIAL CONDITION DEPENDENCE

In the overdamped limit, the infinitesimal heat and work in (4) during the time interval dt are given by, respectively, $đQ_1=-f_1\circ dx_1=-f_1^2dt-f_1\circ d\Xi_1$ and $đW=-\boldsymbol{f}_{nc}\circ d\boldsymbol{x}=-(\boldsymbol{f}_{nc}\cdot\boldsymbol{f})dt-f_{nc,1}\circ d\Xi_1-f_{nc,2}\circ d\Xi_2$ (γ is set to 1). We use $\cdot$ for the inner product of a vector with another vector or a matrix. Hence, $\boldsymbol{y}=(x_1,x_2,Q=Q_1,W)^{\mathsf{T}}$ follows a stochastic differential equation

$$\dot{\boldsymbol{y}}=\boldsymbol{d}+\mathsf{N}\cdot\boldsymbol{\zeta}, \tag{A1}$$

where the drift vector $\boldsymbol{d}=(f_1,f_2,-f_1^2,-\boldsymbol{f}\cdot\boldsymbol{f}_{nc})^{\mathsf{T}}$, the 4×2 noise matrix N is given by

$$\mathsf{N}=\begin{pmatrix}\sqrt{2T_1} & 0\\ 0 & \sqrt{2T_2}\\ -\sqrt{2T_1}f_1 & 0\\ -\sqrt{2T_1}f_{nc,1} & -\sqrt{2T_2}f_{nc,2}\end{pmatrix}, \tag{A2}$$

and the components of the noise vector $\boldsymbol{\zeta}(t)=(\zeta_1(t),\zeta_2(t))^{\mathsf{T}}$ are independent Gaussian random variables of zero mean and unit variance. The total force $\boldsymbol{f}=\boldsymbol{f}_c+\boldsymbol{f}_{nc}$ is linear in $\boldsymbol{x}$, hence it is written as $\boldsymbol{f}=-\mathsf{F}\cdot\boldsymbol{x}$ with the force matrix F.

The differential equation is nonlinear and involves the multiplicative noises implemented with the Stratonovich interpretation. Following the standard recipe [43], one can derive the Fokker-Planck equation for the probability distribution $p(\boldsymbol{y};t)$:

$$\frac{\partial p}{\partial t}=\mathcal{L}p, \tag{A3}$$

where the Fokker-Planck operator is given by

$$\mathcal{L}=-\boldsymbol{\nabla}^{\mathsf{T}}\cdot\boldsymbol{d}+\tfrac{1}{2}(\boldsymbol{\nabla}^{\mathsf{T}}\cdot\mathsf{N})\cdot(\boldsymbol{\nabla}^{\mathsf{T}}\cdot\mathsf{N})^{\mathsf{T}}, \tag{A4}$$

with the differential operator $\boldsymbol{\nabla}=(\frac{\partial}{\partial x_1},\frac{\partial}{\partial x_2},\frac{\partial}{\partial Q},\frac{\partial}{\partial W})^{\mathsf{T}}$.

For $G(x_1,x_2,\lambda_Q,\lambda_W;t)$ defined in (18), the time evolution operator $\mathcal{L}_\lambda$ is obtained by replacing $\partial/\partial Q$ and $\partial/\partial W$ in $\mathcal{L}$

with λ_Q and λ_W, respectively. The resulting operator becomes bilinear in $\boldsymbol{x}$ and the gradient operator $\boldsymbol{\nabla}_{\boldsymbol{x}} = (\frac{\partial}{\partial x_1}, \frac{\partial}{\partial x_2})^{\mathsf{T}}$, i.e.,

$$\mathcal{L}_\lambda = \boldsymbol{\nabla}_{\boldsymbol{x}}^{\mathsf{T}} \cdot \mathsf{D} \cdot \boldsymbol{\nabla}_{\boldsymbol{x}} + 2\boldsymbol{x}^{\mathsf{T}} \cdot \mathsf{B}^{\mathsf{T}} \cdot \boldsymbol{\nabla}_{\boldsymbol{x}} + \boldsymbol{x}^{\mathsf{T}} \cdot \mathsf{A} \cdot \boldsymbol{x} + K + \mathrm{Tr}\mathsf{B}, \tag{A5}$$

where A and $\mathsf{D} = \mathrm{diag}(T_1, T_2)$ are the 2×2 symmetric matrices, B is the 2×2 nonsymmetric matrix, and $\mathrm{Tr}\mathsf{X}$ denotes the trace of a matrix X. The matrix elements for A and B are readily obtained from (A4). Explicitly, they are given by $\mathsf{A} = \mathsf{C}^{\mathsf{T}}\mathsf{D}\mathsf{C} + \frac{1}{2}\mathsf{F}^{\mathsf{T}}\mathsf{C} + \frac{1}{2}\mathsf{C}^{\mathsf{T}}\mathsf{F}$ and $\mathsf{B} = \mathsf{D}\mathsf{C} + \frac{1}{2}\mathsf{F}$ with an auxiliary matrix

$$\mathsf{C} = \begin{pmatrix} K\lambda_Q & -\epsilon(\lambda_Q + \lambda_W) \\ -\delta\lambda_W & 0 \end{pmatrix}. \tag{A6}$$

We now rescale the coordinates to define $\hat{\boldsymbol{x}} = (\hat{x}_1, \hat{x}_2)^{\mathsf{T}} \equiv \mathsf{D}^{-1/2} \cdot \boldsymbol{x}$. Then the time evolution operator is rewritten in terms of $\hat{\boldsymbol{x}}$ as

$$\mathcal{L}_\lambda = \nabla_{\hat{\boldsymbol{x}}}^2 + 2\hat{\boldsymbol{x}}^{\mathsf{T}} \cdot \hat{\mathsf{B}}^{\mathsf{T}} \cdot \boldsymbol{\nabla}_{\hat{\boldsymbol{x}}} + \hat{\boldsymbol{x}}^{\mathsf{T}} \cdot \mathsf{D}\hat{\mathsf{A}} \cdot \hat{\boldsymbol{x}} + K + \mathrm{Tr}\mathsf{B}, \tag{A7}$$

where $\boldsymbol{\nabla}_{\hat{\boldsymbol{x}}} = (\frac{\partial}{\partial \hat{x}_1}, \frac{\partial}{\partial \hat{x}_2})^{\mathsf{T}}$ and $\hat{\mathsf{X}} = \mathsf{D}^{-1/2} \cdot \mathsf{X} \cdot \mathsf{D}^{1/2}$ for any matrix X. It looks similar to the Hamiltonian of the two-dimensional harmonic oscillator except for the second term. Finally, we make a transformation

$$\widetilde{\mathcal{L}}_\lambda \equiv e^{(1/2)\hat{\boldsymbol{x}}^{\mathsf{T}} \cdot \mathsf{J} \cdot \hat{\boldsymbol{x}}} \mathcal{L}_\lambda e^{-(1/2)\hat{\boldsymbol{x}}^{\mathsf{T}} \cdot \mathsf{J} \cdot \hat{\boldsymbol{x}}}, \tag{A8}$$

with a certain symmetric matrix J, which will be determined later. It acts as the time evolution operator for the modified generating function $e^{(1/2)\boldsymbol{x}^{\mathsf{T}} \cdot \mathsf{D}^{-1/2}\mathsf{J}\mathsf{D}^{-1/2} \cdot \boldsymbol{x}} G(\boldsymbol{x}, \lambda_Q, \lambda_W; t)$. This transformation replaces the gradient operator $\boldsymbol{\nabla}_{\hat{\boldsymbol{x}}}$ with $\boldsymbol{\nabla}_{\hat{\boldsymbol{x}}} - \mathsf{J} \cdot \hat{\boldsymbol{x}}$, which leads to

$$\widetilde{\mathcal{L}}_\lambda = \nabla_{\hat{\boldsymbol{x}}}^2 - 2\hat{\boldsymbol{x}}^{\mathsf{T}} \cdot \mathsf{M}^{\mathsf{T}} \cdot \boldsymbol{\nabla}_{\hat{\boldsymbol{x}}} + \hat{\boldsymbol{x}}^{\mathsf{T}} \cdot \mathsf{Q} \cdot \hat{\boldsymbol{x}} + \mu, \tag{A9}$$

where

$$\begin{aligned} \mathsf{M} &= \mathsf{J} - \hat{\mathsf{B}}, \\ \mathsf{Q} &= \mathsf{M}^{\mathsf{T}}\mathsf{M} + \mathsf{D}\hat{\mathsf{A}} - \hat{\mathsf{B}}^{\mathsf{T}}\hat{\mathsf{B}} = \mathsf{M}^{\mathsf{T}}\mathsf{M} - \tfrac{1}{4}\hat{\mathsf{F}}^{\mathsf{T}}\hat{\mathsf{F}}, \\ \mu &= K - \mathrm{Tr}\mathsf{M}. \end{aligned} \tag{A10}$$

The operator $\widetilde{\mathcal{L}}_\lambda$ is simplified if one chooses J or M suitably so that $\mathsf{Q} = 0$. It is accomplished by choosing

$$\mathsf{J} = \hat{\mathsf{B}} + \tfrac{1}{2}\mathsf{O}\hat{\mathsf{F}}, \tag{A11}$$

with an orthogonal matrix

$$\mathsf{O} = \begin{pmatrix} \cos\theta & -\sin\theta \\ \sin\theta & \cos\theta \end{pmatrix}. \tag{A12}$$

The angle variable θ has to be determined by requiring that J should be a symmetric matrix. Then the time evolution operator $\widetilde{\mathcal{L}}_\lambda$ has the constant eigenfunction with the corresponding eigenvalue μ. As a result, in the large t limit, the generating function G has the asymptotic form in (19).

We find that the symmetry condition $J_{12} = J_{21}$ is satisfied if

$$\theta = \alpha \pm \beta, \tag{A13}$$

where $\cos\alpha = \frac{\hat{F}_{12} - \hat{F}_{21}}{R}$, $\sin\alpha = -\frac{\hat{F}_{11} + \hat{F}_{22}}{R}$, $\cos\beta = \frac{2(\hat{B}_{21} - \hat{B}_{12})}{R}$, and $\sin\beta = \sqrt{1 - \cos^2\beta}$ with

$$R = \sqrt{(\hat{F}_{12} - \hat{F}_{21})^2 + (\hat{F}_{11} + \hat{F}_{22})^2}. \tag{A14}$$

There are two different solutions for J due to the sign ambiguity in (A13). To select the proper solution, we impose the condition that the generating function $G(\boldsymbol{x}, \lambda_Q, \lambda_W; t)$ in the infinite t limit should converge to the steady-state distribution when $\lambda_Q = \lambda_W = 0$. The steady-state probability distribution of a linear system is known exactly [39]. Comparing the two solutions with the steady-state probability distribution, we find that the matrix J is indeed given by $\mathsf{J} = \hat{\mathsf{B}} + \frac{1}{2}\mathsf{O}\hat{\mathsf{F}}$ with $\theta = \alpha + \beta$. The eigenvalue is given by

$$\mu(\lambda_Q, \lambda_W) = K - \frac{R}{2}\sin\beta, \tag{A15}$$

which yields the result in (20).

We add a remark on the initial condition dependence. As for the effect of the initial condition, Visco studied a similar problem, a Brownian particle in one dimension in contact with two heat baths [50]. One can apply the same method in Ref. [50] to study the initial condition dependence. Suppose that initial state $\boldsymbol{x}_0$ of the system at time $t = 0$ is distributed according to a probability distribution $p_0(\boldsymbol{x}_0)$. Then the moment generating function G_t in (19) should be integrated over the initial position $\boldsymbol{x}_0$ after being multiplied with the additional factor $r(\boldsymbol{x}_0, \lambda_Q, \lambda_W)$ that is determined by the initial distribution and the leading eigenstate of the Fokker-Planck operator $\widetilde{\mathcal{L}}_\lambda$. Just as the integration over $\boldsymbol{x}$ introduces the branch cut represented by the curve C in Fig. 4, the integration over $\boldsymbol{x}_0$ can also introduces a branch cut. When the additional branch cut shrinks the analytic domain in Fig. 4, the efficiency LDF $L(\eta)$ becomes broader. We do not have the analytic expression for the eigenfunction of the Fokker-Planck operator yet. Instead, we investigate the initial condition dependence numerically. In Fig. 5 we compare the LDFs from the fixed initial condition and from the steady-state initial condition. One finds that the LDF from the latter displays a broader distribution on the $\eta \geqslant \bar{\eta}$ side.

[1] F. L. Curzon and B. Ahlborn, Am. J. Phys. **43**, 22 (1975).
[2] P. Chambadal, *Les Centrales Nucléaires* (Armand Colin, Paris, 1957).
[3] I. I. Novikov, J. Nucl. Energy II **7**, 125 (1958).
[4] D. P. Sekulic, J. Appl. Phys. **83**, 4561 (1998).
[5] B. Andersen, J. Appl. Phys. **90**, 6557 (2001).
[6] A. Gomez-Marin and J. M. Sancho, Phys. Rev. E **74**, 062102 (2006).
[7] T. Schmiedl and U. Seifert, Europhys. Lett. **81**, 20003 (2008).
[8] Z. C. Tu, J. Phys. A: Math. Theor. **41**, 312003 (2008).

[9] Y. Izumida and K. Okuda, Europhys. Lett. **83**, 60003 (2008).
[10] Y. Izumida and K. Okuda, Phys. Rev. E **80**, 021121 (2009).
[11] Y. Izumida and K. Okuda, Prog. Theor. Phys. Suppl. **178**, 163 (2009).
[12] M. Esposito, K. Lindenberg, and C. Van den Broeck, Europhys. Lett. **85**, 60010 (2009).
[13] M. Esposito, R. Kawai, K. Lindenberg, and C. Van den Broeck, Phys. Rev. E **81**, 041106 (2010).
[14] M. Esposito, N. Kumar, K. Lindenberg, and C. Van den Broeck, Phys. Rev. E **85**, 031117 (2012).
[15] Y. Apertet, H. Ouerdane, C. Goupil, and P. Lecoeur, Phys. Rev. E **85**, 031116 (2012).
[16] Y. Apertet, H. Ouerdane, C. Goupil, and P. Lecoeur, Phys. Rev. E **85**, 041144 (2012).
[17] C. Van den Broeck and K. Lindenberg, Phys. Rev. E **86**, 041144 (2012).
[18] T. Schmiedl and U. Seifert, Europhys. Lett. **83**, 30005 (2008).
[19] Y. Zhou and D. Segal, Phys. Rev. E **82**, 011120 (2010).
[20] U. Seifert, Phys. Rev. Lett. **106**, 020601 (2011).
[21] N. Golubeva, A. Imparato, and L. Peliti, Europhys. Lett. **97**, 60005 (2012).
[22] C. Van den Broeck, N. Kumar, and K. Lindenberg, Phys. Rev. Lett. **108**, 210602 (2012).
[23] N. Golubeva and A. Imparato, Phys. Rev. Lett. **109**, 190602 (2012).
[24] N. Golubeva and A. Imparato, Phys. Rev. E **88**, 012114 (2013).
[25] H. Hooyberghs, B. Cleuren, A. Salazar, and J. O. Indekeu, J. Chem. Phys. **139**, 134111 (2013).
[26] N. Golubeva and A. Imparato, Phys. Rev. E **89**, 062118 (2014).
[27] A. E. Allahverdyan, R. S. Johal, and G. Mahler, Phys. Rev. E **77**, 041118 (2008).
[28] S. Abe, Phys. Rev. E **83**, 041117 (2011).
[29] P. Muratore-Ginanneschi and K. Schwieger, Phys. Rev. E **90**, 060102 (2014).
[30] P. Muratore-Ginanneschi and K. Schwieger, Europhys. Lett. **112**, 20002 (2015).
[31] S. Sheng and Z. C. Tu, Phys. Rev. E **89**, 012129 (2014).
[32] S. Sheng and Z. C. Tu, Phys. Rev. E **91**, 022136 (2015).
[33] C. Van den Broeck, Phys. Rev. Lett. **95**, 190602 (2005).
[34] M. Esposito, K. Lindenberg, and C. Van den Broeck, Phys. Rev. Lett. **102**, 130602 (2009).
[35] B. Cleuren, B. Rutten, and C. Van den Broeck, Eur. Phys. J. Spec. Top. **224**, 879 (2015).
[36] G. Verley, M. Esposito, T. Willaert, and C. Van den Broeck, Nat. Commun. **5**, 4721 (2014).
[37] G. Verley, T. Willaert, C. Van den Broeck, and M. Esposito, Phys. Rev. E **90**, 052145 (2014).
[38] C. Kwon, P. Ao, and D. Thouless, Proc. Natl. Acad. Sci. USA **102**, 13029 (2005).
[39] C. Kwon, J. D. Noh, and H. Park, Phys. Rev. E **83**, 061145 (2011).
[40] J. D. Noh, C. Kwon, and H. Park, Phys. Rev. Lett. **111**, 130601 (2013).
[41] H.-M. Chun and J. D. Noh, Phys. Rev. E **91**, 052128 (2015).
[42] K. Sekimoto, Prog. Theor. Phys. Suppl. **130**, 17 (1998).
[43] H. Risken and T. Frank, *The Fokker-Planck Equation*, Springer Series in Synergetics Vol. 18 (Springer, Berlin, 1996).
[44] C. Gardiner, *Stochastic Methods*, Springer Series in Synergetics Vol. 13 (Springer, Berlin, 2010).
[45] Z. Rieder, J. Math. Phys. **8**, 1073 (1967).
[46] T. Tomé and M. J. de Oliveira, Phys. Rev. E **82**, 021120 (2010).
[47] E. Lippiello, M. Baiesi, and A. Sarracino, Phys. Rev. Lett. **112**, 140602 (2014).
[48] A. De Vos, Am. J. Phys. **53**, 570 (1985).
[49] A. Bejan, Int. J. Heat Mass Transfer **31**, 1211 (1988).
[50] P. Visco, J. Stat. Mech. (2006) P06006.
[51] A. Greiner, W. Strittmatter, and J. Honerkamp, J. Stat. Phys. **51**, 95 (1988).
[52] K. Proesmans, B. Cleuren, and C. Van den Broeck, Europhys. Lett. **109**, 20004 (2015).
[53] K. Proesmans and C. Van den Broeck, New J. Phys. **17**, 065004 (2015).
[54] J. S. Lee, C. Kwon, and H. Park, Phys. Rev. E **87**, 020104 (2013).
[55] R. García-García, V. Lecomte, A. Kolton, and D. Domínguez, J. Stat. Mech. (2012) P02009.
[56] R. García-García, D. Domínguez, V. Lecomte, and A. B. Kolton, Phys. Rev. E **82**, 030104 (2010).
[57] J. D. Noh and J.-M. Park, Phys. Rev. Lett. **108**, 240603 (2012).
[58] J. D. Noh, J. Stat. Mech. (2014) P01013.
[59] T. Nemoto, Phys. Rev. E **85**, 061124 (2012).
[60] R. van Zon and E. G. D. Cohen, Phys. Rev. Lett. **91**, 110601 (2003).
[61] M. Polettini, G. Verley, and M. Esposito, Phys. Rev. Lett. **114**, 050601 (2015).
[62] J.-H. Jiang, B. K. Agarwalla, and D. Segal, Phys. Rev. Lett. **115**, 040601 (2015).